Journal of Advanced Research 30 (2021) 185–196

Contents lists available at ScienceDirect

Journal of Advanced Research

journal homepage: www.elsevier.com/locate/jare

RBC-derived vesicles as a systemic delivery system of doxorubicin for lysosomal-mitochondrial axis-improved cancer therapy

Shu-Hui Wu [a], Chia-Chu Hsieh [a], Szu-Chun Hsu [b], Ming Yao [c], Jong-Kai Hsiao [d,e], Shih-Wei Wang [f], Chih-Peng Lin [g], Dong-Ming Huang [a,*]

[a] Institute of Biomedical Engineering and Nanomedicine, National Health Research Institutes, Miaoli 35053, Taiwan
[b] Department of Laboratory Medicine, National Taiwan University Hospital and College of Medicine, National Taiwan University, Taipei 100225, Taiwan
[c] Department of Internal Medicine, National Taiwan University Hospital and College of Medicine, National Taiwan University, Taipei 100225, Taiwan
[d] Department of Medical Imaging, Taipei Tzu Chi General Hospital, Buddhist Tzu-Chi Medical Foundation, New Taipei City 23142, Taiwan
[e] School of Medicine, Tzu Chi University, Hualien 97004, Taiwan
[f] Department of Medicine, Mackay Medical College, New Taipei City 252005, Taiwan
[g] Department of Anesthesiology, National Taiwan University Hospital and College of Medicine, National Taiwan University, Taipei 100225, Taiwan

GRAPHICAL ABSTRACT

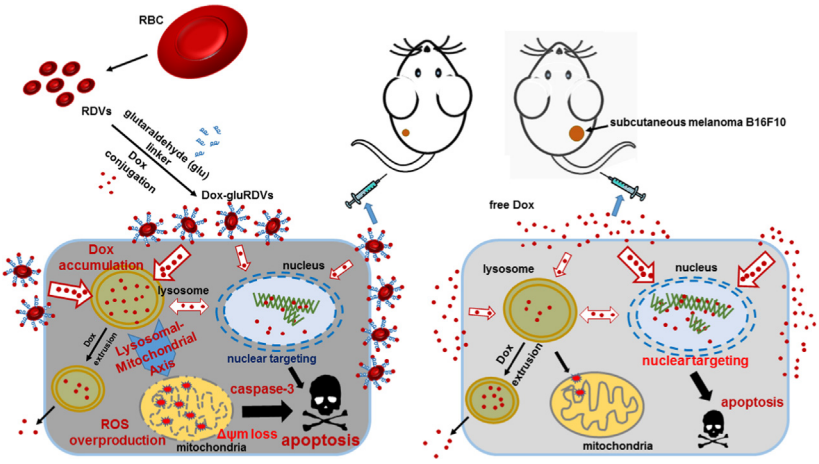

ARTICLE INFO

Article history:
Received 10 July 2020
Revised 19 November 2020
Accepted 22 November 2020
Available online 24 November 2020

Keywords:
Drug delivery
Doxorubicin
Cancer chemotherapy

ABSTRACT

Introduction: Chemotherapeutic drugs are the main intervention for cancer management, but many drawbacks impede their clinical applications. Nanoparticles as drug delivery systems (DDSs) offer much promise to solve these limitations.
Objectives: A novel nanocarrier composed of red blood cell (RBC)-derived vesicles (RDVs) surface-linked with doxorubicin (Dox) using glutaraldehyde (glu) to form Dox-gluRDVs was investigated for improved cancer therapy.
Methods: We investigated the *in vivo* antineoplastic performance of Dox-gluRDVs through intravenous (*i.v.*) administration in the mouse model bearing subcutaneous (*s.c.*) B16F10 tumor and examined the *in vitro* antitumor mechanism and efficacy in a panel of cancer cell lines.

Peer review under responsibility of Cairo University.
* Corresponding author at: Institute of Biomedical Engineering and Nanomedicine, National Health Research Institutes, Miaoli 35053, Taiwan.
E-mail address: dmhuang@nhri.edu.tw (D.-M. Huang).

https://doi.org/10.1016/j.jare.2020.11.009
2090-1232/

Nanoparticle
Lysosome
Mitochondria

Results: Dox-gluRDVs can exert superior anticancer activity than free Dox *in vitro* and *in vivo*. Distinct from free Dox that is mainly located in the nucleus, but instead Dox-gluRDVs release and efficiently deliver the majority of their conjugated Dox into lysosomes. In vitro mechanism study reveals the critical role of lysosomal Dox accumulation-mediated mitochondrial ROS overproduction followed by the mitochondrial membrane potential loss and the activation of apoptotic signaling for superior anticancer activity of Dox-gluRDVs.
Conclusion: This work demonstrates the great potential of RDVs to serve a biological DDS of Dox for systemic administration to improve conventional cancer chemotherapeutics.

Introduction

Despite many efforts have been made in the development of cancer treatment, chemotherapy remains the main intervention for cancer management. However, the use of chemotherapeutic drugs is often limited by several drawbacks such as poor solubility, non-specific distribution between cancer cells and non-cancer cells, rapid elimination, and the inaccessibility to cancer cells. In this regard, nanotechnology has drawn attention as one of the most promising approaches for an effective and specific chemotherapy in cancer management. Many biomaterials have been used to construct nanoplatforms as drug delivery systems (DDSs) [1]. DDSs can be artificially made from synthetic or natural components, and therefore these artificial DDSs (aDDSs) possess advantages of rational design, diversity, and feasible manipulation of materials [2] but an inherent disadvantage of clinical biocompatibility hazard as well. In contrast, biological DDSs (bDDSs) composed of natural cells and their segments demonstrate much better biocompatibility and natural biofunctions. In addition, hybrid DDSs (hDDSs) are developed to theoretically combine advantages of aDDSs and bDDSs while alleviating their shortcomings [2,3].

Red blood cells (RBCs) with many biological advantages are most frequently explored as a source for bDDSs [2,3]. However, the size of these carrier RBCs in the micrometer level limits the accessibility of carrier RBCs with their cargos to extravascular targets, including tumors [4]. Lejeune et al. first reported the preparation of sub-micron vesicles named nanoerythrosomes (nEryt) by physical extrusion of RBC ghost membranes. In a mouse model intraperitoneally bearing P388D1 leukemia tumor, the daunorubicin (DNR)-conjugated nEryt (nEryt-DNR) at higher concentration of DNR showed better antineoplastic activity than free DNR via intraperitoneal (*i.p.*) injection [5]. Theoretically, nEryt could reach RBC-inaccessible target sites including tumors; however, systemic antineoplastic studies, i.e. intravenous (*i.v.*) administration of nEryt, of this bDDS had not been proceeded *in vivo*, perhaps due to a rapid clearance from blood circulation [6] as nEryt lost the biocompatibility during preparation process [7]. For nEryt and other bDDSs that are entirely cell-based [3], the direct drug loading might further affect their stability and biocompatibility. Recently, the hDDS system of using RBC membranes to camouflage synthetic nanoparticles have been demonstrated to practice *in vivo* biomedical applications including anticancer therapies [8,9]. However, potential hazards associated with xenogeneic nanomaterials are largely pending once their RBC cloaks are degraded.

We have developed a novel nanocarrier composed of RBC-derived vesicles (RDVs) that could efficiently encapsulate protoporphyrin IX (PpIX), and the as-synthesized PpIX-encapsulated RDVs (PpIX@RDVs) showed highly phototoxic effect in Huh7 cells upon irradiation *in vitro* [10]. Our previous studies suggest that RDVs possessing sufficient stability and biocompatibility could be a facile and effective bDDS for systemically administered cancer therapy [10,11].

In the present study, therefore, we bound the antitumor drug doxorubicin (Dox) onto RDVs with glutaraldehyde (glu) linker as previously reported [5], resulting in the synthesis of Dox-conjugated RDVs (Dox-gluRDVs). We investigated the *in vivo* antineoplastic performance of Dox-gluRDVs through *i.v.* administration in the mouse model bearing subcutaneous (*s.c.*) B16F10 tumor and examined the *in vitro* antitumor mechanism and efficacy in a panel of cancer cell lines between Dox-gluRDVs and free Dox to explore the potential of RDVs for being a bDDS for conventional cancer chemotherapy.

Materials and methods

Preparation and characterization of Dox-gluRDVs

Blood samples of were collected from healthy regular donors with informed consent approved according to the procedures of the institutional review board of the National Health Research Institutes (NHRI), Taiwan (EC1031204). The preparation of RDVs was performed as previously described [11]. Briefly, blood cell sediments were mixed with a gradient of CaCl2 (1 M) and EDTA (390 mM) at 45 °C for 30 min, followed by centrifuging at 1,700 g at 4 °C for 10 min. RDVs were harvested by centrifugation at 16,000 g at 4 °C for 10 min, and resuspended in Dulbecco's phosphate buffered saline (DPBS, GIBCO). RDVs generated from three randomized donors' blood samples were pooled and used in each single experiment. For the synthesis of Dox-gluRDVs or gluRDVs, RDVs were lysed in 5% SDS and Bradford Protein Assay (Bio-Rad) was used to determine the protein concentration of RDVs. RDVs (2 mg) was incubated with Dox (ENZO life science) (400 μg) or not in the presence of 0.05% glutaraldehyde (EMS) in a final volume of 2 mL in PBS at 37 °C for 30 min and the reaction was stopped by the addition of 0.3 mL of 15% glycine (Sigma). DOX-gluRDVs or gluRDVs was collected by centrifugation at 16,000 g for 10 min at room temperature with PBS wash for 3 times. The conjugation of Dox with gluRDVs may vary depending on donors and their RBC statuses. To determine the conjugation efficiency, DOX-gluRDVs pellets were incubated with lysis buffer (5% SDS), and the solution was then examined spectrophotometrically at 570 nm using a microplate reader (SpectraMAX M2, Molecular Device). The conjugated Dox content was calculated from a standard plot of known concentrations of free Dox vs. the corresponding absorbance density. The particle size and zeta pontential of RDVs, gluRDVs, and Dox-gluRDVs were determined by Nano ZS (Malvern). The particle size and the surface potential quite vary depending on donors and their RBC statuses. The morphology was determined by Hitachi H-7650 Transmission Electron Microscope (TEM) at 100 kV. To determine the protein contents, RDVs or RBCs were lysed using RDV lysis buffer containing 1.5 M ammonium chloride, 10 μM sodium bicarbonate, 12 μM EDTA (all from Sigma) and the protein concentration was determined by Bradford Protein Assay. The protein samples were separated by elec-

trophoresis in a 10% polyacrylamide gel and transferred to PVDF membrane. The membranes were incubated with TBS plus 0.1% Tween 20 (TBST) and 5% bovine serum albumin (BSA) for 1 h at room temperature. After incubation, primary antibodies (Band3, dilution 1:1000, Santa Cruz; Stomatin, dilution 1:1000, Santa Cruz; Flotillin1, dilution 1:1000, Santa Cruz; Flotillin2, dilution 1:1000, Santa Cruz; Hemoglobin, dilution 1:5000, Santa Cruz; β-actin, dilution 1:10000, Santa Cruz) were added to TBST containing 1% BSA and incubated with the membranes at 4 ℃ overnight. The membranes were then incubated with HRP-conjugated secondary antibodies (dilution 1:5000, Santa Cruz) and were developed using the Luminata Cresendo Western HRP substrate (Millipore).

Cell culture

Murine melanoma B16F10 cells were cultured in high-glucose DMEM, human colon adenocarcinoma HT-29 cells, human uterine sarcoma MES-SA cells and MES-SA/DX5 cells were cultured in McCoy's 5A medium, human prostate adenocarcinoma PC3 cells were cultured in low-glucose DMEM, and human ovary adenocarcinoma TOV21G cells were cultured in RPMI1640. All media were purchased from GIBCO and supplemented with 10% fetal bovine serum (FBS) (FetalEqual), 100 U/mL of penicillin, and 100 μg/mL of streptomycin (GIBCO). All cultures were maintained in a 5% CO2 atmosphere at 37 °C.

In vitro cytotoxicity assay

Cells (1×10^4 cells) were seeded in a 96-well plate and allowed to attach for 24 h, and then treated with free Dox or Dox-gluRDVs at the indicated Dox concentrations, or with gluRDVs at the proportional concentrations to Dox-gluRDVs in growth media for 24 h. To evaluate the role of reactive oxygen species (ROS) in the cytotoxicity, in some experiments cells were pretreated with N-acetylcysteine (NAC, Sigma) at 5 mM for 2 h before the treatments of gluRDVs, free Dox or Dox-gluRDVs. The cell viability was determined using 3-[4,5-dimethylthiazol-2-yl] −2,5-diphenyltetrazolium bromide (MTT) reduction assay by microplate reader (SpectraMAX M2, Molecular Device). The data are expressed as the percentage variation of control cell viability as 100%.

In vivo anticancer activity assay

Six-week-old female C57BL/6 were purchased from the National Laboratory Animal Center of Taiwan and housed under specific pathogen-free conditions and with a 12 h light/12 h dark cycle. Mice were injected subcutaneously in the right flank with 5×10^5 B16F10 murine melanoma cancer cell suspended in 100 μL of PBS. At day 12 and day 19 post the cancer cell inoculation, mice were injected with vehicle (control, n = 4), gluRDVs (n = 6), free Dox (0.5 mg/kg, n = 5 or 5 mg/kg, n = 5), or Dox-gluRDVs (0.1 mg/kg of Dox, n = 6) through the lateral tail vein. Tumor volume was measured by caliper and calculated according to the formula: volume = length × width^2/2. Animal experiments were carried out according to the guidelines of the Institutional Animal Care and Use Committee (IACUC) of NHRI (NHRI-IACUC) and performed after receiving approval from NHRI-IACUC (104143-A).

Intracellular Dox distribution and ROS generation

To observe the intracellular distribution of Dox, cells were seeded in a μ-Slides 8 Well (IBIDI) (2×10^4 cells per well) and allowed to attach overnight, and then treated with free Dox or Dox-gluRDVs at 10 μM Dox for 1 h at 37 °C, followed by PBS wash. Fresh media containing 50 nM LysoTracker Blue DND-22 (Molecular Probes) were added and incubated for 20 min. The cells were washed with PBS and observed with TCS SP5 confocal microscope (Leica) using a 63x oil immersion objective. Todetermine the intracellular ROS generation, cells were seeded in 6-well plate (2×10^5 cells per well) and allowed to attach for 24 h, and then pretreated with N-acetylcysteine (NAC at 5 mM) or not (CTL) for 2 h, followed by the treatment with vehicle (control), gluRDVs at the proportional concentrations to Dox-gluRDVs, free Dox, or Dox-gluRDVs at 1 μM Dox for 24 h at 37 °C. The cells were washed and incubated with 10 mM 2′,7′-Dichlorofluorescin diacetate (DCFDA, Sigma) for 20 min, and then trypsinized and collected with DPBS on ice for flow cytometry analysis.

Lysosomal Dox accumulation and mitochondrial ROS generation

To distinguish between lysosomal Dox and ROS location, cells were seeded in a μ-Slides 8 Well (IBIDI) (2×10^4 cells per well) and allowed to attach for overnight, treated with free Dox or Dox-gluRDVs at 10 μM Dox for the indicated times at 37 °C, and then washed and incubated with 10 mM DCFDA for 20 min. After PBS wash, cells were then stain with 50 nM LysoTracker Blue DND-22 and 20 nM MitoTracker Deep Red for 20 min and observed with TCS SP5 confocal microscope.

Measurement of mitochondrial membrane potential ($\Delta\psi m$)

$\Delta\psi m$ was determined using Rhodamine-123 (Rh-123, Sigma) staining. Cells were seeded in either 6-well plate (2×10^5 cells per well) for flow cytometry analysis or μ-Slides 8 Well (2×10^4 cells per well) for microscopic observation, and allowed to attach for 24 h. After treatment with vehicle (control), gluRDVs at the proportional concentrations to Dox-gluRDVs, free Dox, Dox-gluRDVs at 10 μM Dox, or carbonyl cyanide 4-(trifluoromethoxy) phenylhydrazone (FCCP at 100 μM, Sigma) as positive control for 8 h, cells were incubated with 2 μg/mL Rh-123 for 5 min in the dark. Cells in 6-well plate were collected by trypsinization in DPBS on ice for flow cytometry. In addition, cells seeded in μ-Slides 8 Well were stained with 10 μg/mL Hoechst33342 (Sigma) for 5 min in the dark and then observed with TCS SP5 confocal microscope.

Western blot analysis

Cells (1×10^5 cells) were seeded in 2 mL growth medium in a 3-cm dish. Following a 24-h incubation period at 37 ℃, cells were treated with vehicle (control), gluRDVs at the proportional concentrations to Dox-gluRDVs, free Dox, and Dox-gluRDVs at 0.3 μM Dox in growth media for 24 h, lysed using RIPA lysis buffer, centrifuged to collect the supernatants, and the protein concentration was determined by Bradford Protein Assay. The protein samples were separated by electrophoresis in a 10% polyacrylamide gel and transferred to PVDF membrane. The membranes were incubated with TBS plus 0.1% Tween 20 (TBST) and 5% bovine serum albumin (BSA) for 1 h at room temperature. After incubation, primary antibodies (ERK, dilution 1:500, Santa Cruz; p-ERK, dilution 1:500, Santa Cruz; Procaspase-3, dilution 1:1000, Cell signaling; Cleaved caspase-3, dilution 1:500, Cell signaling; GAPDH, dilution 1:10000, Santa Cruz) were added to TBST containing 1% BSA and incubated with the membranes at 4 ℃ overnight. The membranes were then incubated with HRP-conjugated secondary antibodies (dilution 1:5000, Santa Cruz) and were developed using the Luminata Cresendo Western HRP substrate (Millipore).

Statistical analysis

Data are presented as the mean ± standard error of mean (SEM) for the indicated numbers of separate experiments. The results

were compared using Student's *t*-test in case of two groups for comparison. Statistical significance was assigned if the probability value (p) was<0.05.

Results and discussions

Synthesis and characterization of Dox-conjugated RDVs (Dox-gluRDVs)

The features of RBC-based bDDS and hDDS may vary due to different preparation processes as well as post-modifications. For example, in contrast to nEryt which were obtained by extrusions of hemoglobin-emptied erythrocyte ghosts [5] as most RBC-based bDDS and hDDS were emptied of their hemoglobin, our RDVs generated from $CaCl_2$/EDTA-induced budding of RBCs retained hemoglobin (Hb) to favor photodynamic therapy (PDT) *in vitro* [11]. Also, the components of RBC-based bDDS and hDDS differ from their parent RBCs. As shown in Fig. 1A, band 3, flotillin 2 and stomatin proteins were much more expressed but actin could not be detectable in RDVs compared to RBCs. RDVs expressed less Hb than RBCs. The alterations of features may offer RBC-based bDDS and hDDS diverse pros and cons of systemic interventions. Using glutaraldehyde (glu) as a linker, Dox was conjugated onto the surface of RDVs, and therefore gluRDVs (without Dox conjugation) and Dox-gluRDVs were synthesized. Although the sizes of gluRDVs and Dox-gluRDVs slightly increased, they were highly monodispersed as native RDVs with an average diameter of 296.8 nm in the aqueous solutions, such as phosphate buffered saline and cultured medium, and had average diameters of 359.6 nm and 487.0 nm, respectively (Fig. 1B). The surface charge was not significantly different between RDVs and gluRDVs or Dox-gluRDVs. The zeta potentials of RDVs, gluRDVs or Dox-gluRDVs were about −6.50 ± 0.39, −9.31 ± 0.42 and −10.12 ± 0.89 mV, respectively. Fig. 1C shows the TEM images of RDVs, gluRDVs or Dox-gluRDVs. RDVs, gluRDVs or Dox-gluRDVs were quasi-spherical and displayed no morphological difference, but gluRDVs and Dox-gluRDVs were prone to agglomerate. In the samples from eleven experiments, 33.8 ± 4.1% of loaded Dox (200 μg), about 67.5 μg of Dox, were conjugated with gluRDVs (1 mg).

In vitro cytotoxicity and in vivo anticancer activity of Dox-gluRDVs

The *in vitro* cytotoxicity of Dox-gluRDVs was examined on a panel of cancer cell lines including melanoma B16F10, colon HT-29, uterine sarcoma MES-SA, prostate PC3, and ovarian TOV21G cells using MTT reduction assay. As control, cells were treated with the same amount of gluRDVs as the one used in the Dox-gluRDVs, demonstrating no observed cytotoxic effects of gluRDVs on these cancer cell lines, except that gluRDVs at higher concentrations had a little cytotoxic effects on B16F10 cells (Fig. 2A) since possibly B16F10 cells were more sensitive to the coverage effect of gluRDVs on cell surface. There was no significant cytotoxicity difference between free Dox and gluRDVs/free Dox in all tested cancer cell

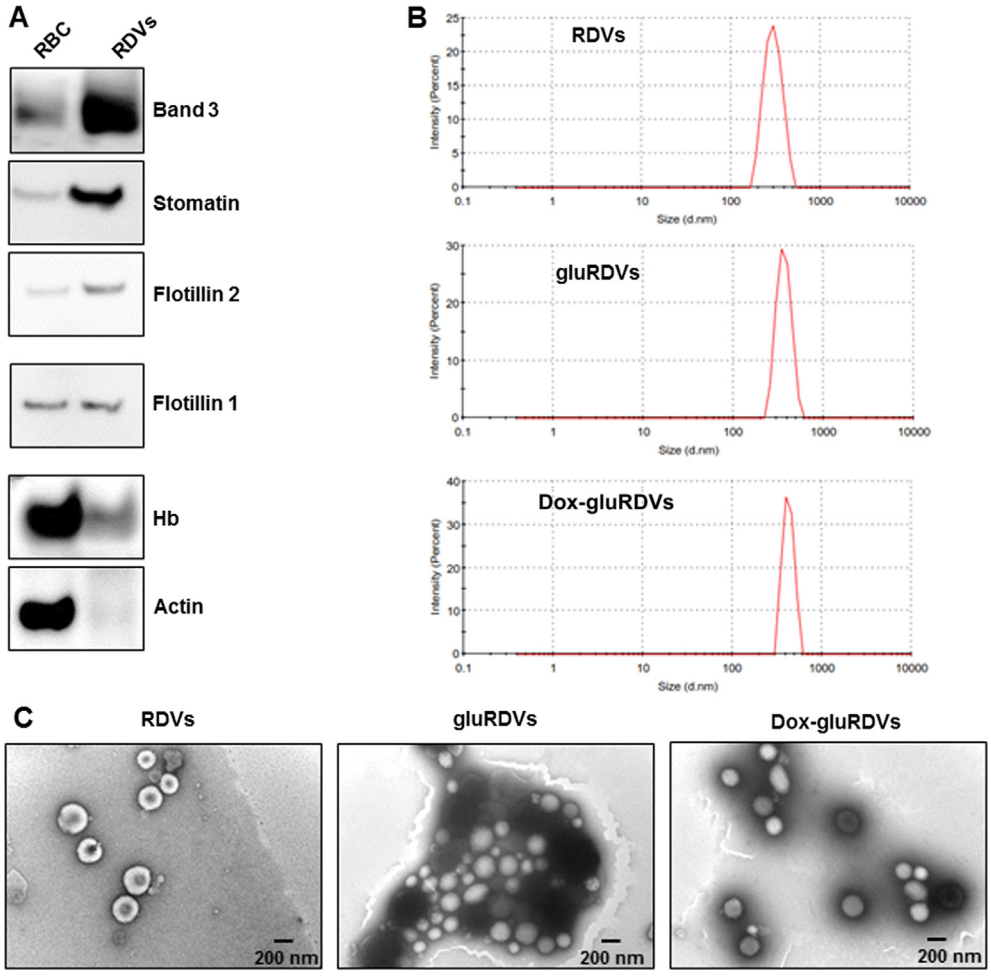

Fig. 1. Characterization of RDVs and Dox-gluRDVs. (A) The different profile of protein component in RBCs and RDVs. (B) Particle-size distribution of RDVs, gluRDVs, and Dox-gluRDVs. (C) TEM image of RDVs, gluRDVs, and Dox-gluRDVs.

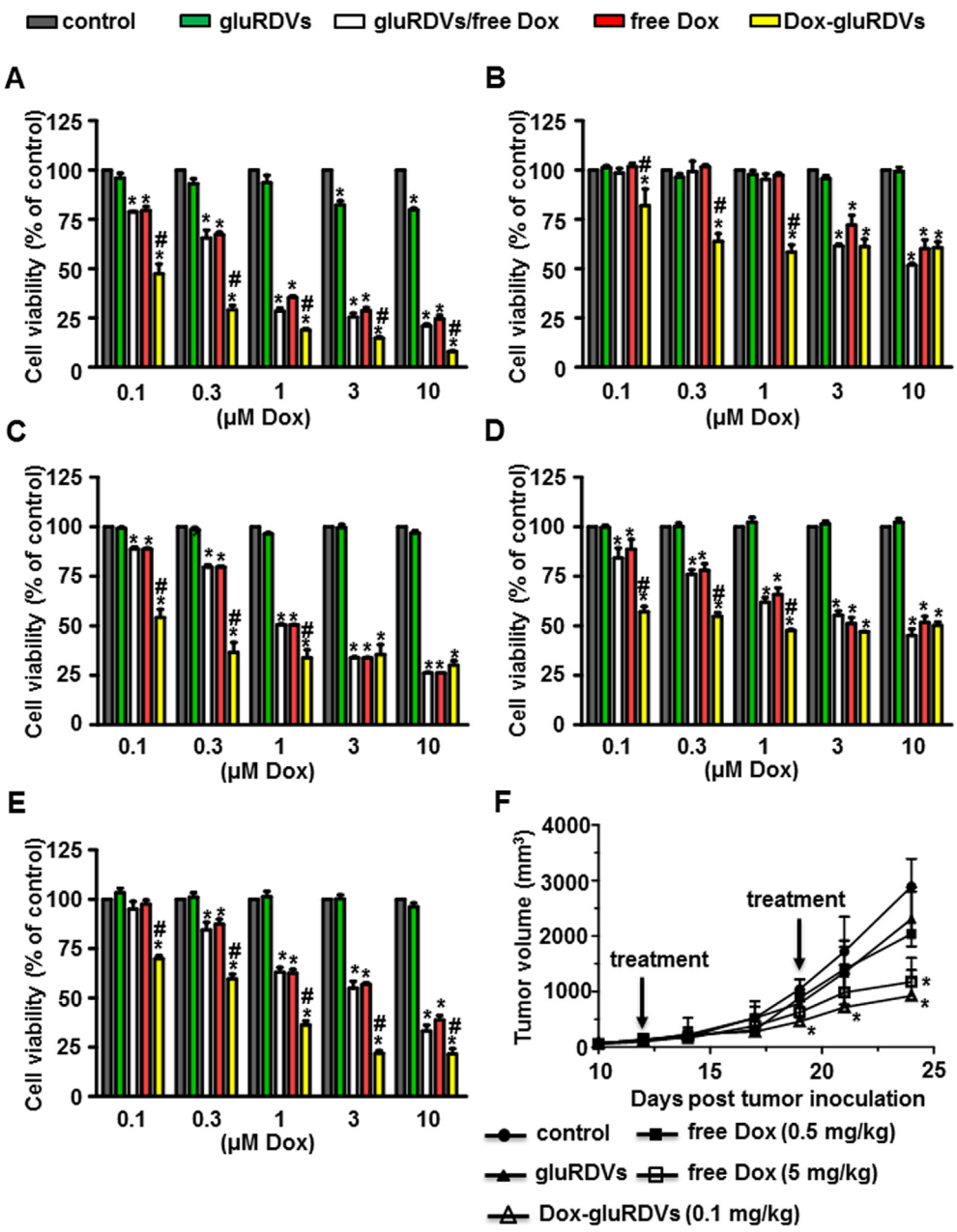

Fig. 2. In vitro cytotoxicity and *in vivo* anticancer activity of Dox-gluRDVs. (A–E) These cells, including B16F10 cells (A), HT-29 cell (B), MES-SA cells (C), PC3 cells (D), and TOV21G cells (E), were incubated for 24 h with increasing antitumor drug concentrations of free Dox, Dox-gluRDVs or a mixture of gluRDVs and free Dox without conjugation procedure (gluRDVs/free Dox) and then processed for MTT cell viability assay (p-values: * < 0.05 as compared with control; # < 0.05 as compared with free Dox). (F) Tumor growth curves of different groups of B16F10-bearing mice (n = 4 to 6 mice per group) (p-values: * < 0.05 as compared with control). At the low concentration of free Dox used (0.5 mg/kg), Dox did not show significant tumor growth inhibition while the antitumor activity of Dox was significantly elevated at high concentration of 5 mg/kg as compared to control. To avoid the possibility of immunologic responses by xenogeneic RDVs, Dox-gluRDVs at 0.1 mg/kg of Dox was used by comparison with the same amount of gluRDVs as the one used in the Dox-gluRDVs. At that concentration, gluRDVs did not show inhibitory effect on tumor growth. No difference of animal body weight between groups was observed (data not shown).

lines. As shown in Fig. 2A, free Dox, gluRDVs/free Dox and Dox-gluRDVs showed an onset cytotoxicity at 0.1 μM and dose-dependent cytotoxicity while Dox-gluRDVs were more cytotoxic than free Dox and gluRDVs/free Dox on B16F10 cells at all tested dosages. In HT-29 cells, Dox-gluRDVs showed the significant onset cytotoxicity at 0.1 μM were much more cytotoxic than free Dox and gluRDVs/free Dox at 0.1 μM, 0.3 μM and 1 μM while free Dox and gluRDVs/free Dox had an onset cytotoxicity at 3 μM. However, Dox-gluRDVs were as cytotoxic as free Dox and gluRDVs/free Dox at 3 μM and 10 μM on HT-29 cells (Fig. 2B). In MES-SA cells (Fig. 2C), free Dox, gluRDVs/free Dox and Dox-gluRDVs had an onset cytotoxicity at 0.1 μM. Free Dox and gluRDVs/free Dox showed a dose-dependent cytotoxicity while the cytotoxicity of Dox-gluRDVs was dramatically increased at 0.1 μM but till 0.3 μM and the following higher concentrations. Nevertheless, Dox-gluRDVs exerted more potent cytotoxicity than free Dox and gluRDVs/free Dox in the treated increasing concentrations except 3 μM and 10 μM on MES-SA cells. In Fig. 2D, the cytotoxicity of Dox-gluRDVs was markedly to commence at 0.1 μM but not significantly augmented along with the increasing concentration while the cytotoxicity of free Dox and gluRDVs/free Dox was commenced with less effect at 0.1 μM than Dox-gluRDVs but displayed dose-

dependent cytotoxicity on PC3 cells. Also, Dox-gluRDVs were much more cytotoxic than free Dox at 0.1 μM, 0.3 μM and 1 μM but as cytotoxic as free Dox and gluRDVs/free Dox at 3 μM and 10 μM on PC3 cells. In TOV21G cells, the cytotoxicity of Dox-gluRDVs was to commence at 0.1 μM while the cytotoxicity of free Dox and gluRDVs/free Dox was commenced with a minor effect at 0.3 μM. The cytotoxicity of free Dox, gluRDVs/free Dox and Dox-gluRDVs gradually increased according to their increasing concentration. Still, Dox-gluRDVs were much more cytotoxic than free Dox and gluRDVs/free Dox on TOV21G cells at all tested dosages (Fig. 2E). These results demonstrate that Dox-gluRDVs exert superior antitumor activity than free Dox *in vitro* (Supplementary Fig. S1). Different from nEryt that could only maintain the same antitumor activity of conjugated DNR as the free DNR on P388D1 cells in a long-term incubation condition (72 h) *in vitro* [5] gluRDVs conferred higher antitumor activity on their conjugated Dox on a number of cancer cells in a shorter incubation period (24 h).

Next, the antitumor activity of Dox-gluRDVs was assessed through *i.v.* administration, as demonstrated by tumor size, on *s.c.* melanoma B16F10-bearing mice (Fig. 2F). Surprisingly, Dox-gluRDVs (at 0.1 mg/kg of Dox) exerted equal antitumor activity as free Dox at 5 mg/kg but far more effective antitumor activity than free Dox at 0.5 mg/kg, indicating that gluRDVs could enhance the systemic therapeutic index of Dox. Altogether, the *in vitro* and *in vivo* data indicates the great potential of RDVs for being a systemic bDDS to improve doxorubicin therapeutics for cancer.

To explore the possible mechanism for RDV-enhanced antitumor activity of Dox, *in vitro* flow cytometry was used to examine and compare the cellular uptake efficiency of free Dox and Dox-gluRDVs. However, our results suggested that gluRDVs-enhanced therapeutic index of Dox might not be mediated by the enhancement of short-term uptake inside Dox-gluRDVs-treated cells (Supplementary Figs. S2 and S3).

Intracellular distribution of free Dox and released Dox of Dox-gluRDVs

The mechanistic basis for the cytotoxicity of Dox has been mainly attributed to its nuclear-targeting function, the inhibition of topoisomerase II and DNA intercalation; however, oxidative stress caused by cytoplasmic Dox away from the nuclear DNA has also been known to play a role in the anticancer activity [12–15]. Therefore, using confocal microscopy, we examined the subcellular distribution of Dox in free Dox-treated and Dox-gluRDVs-DiD-treated cancer cells. As shown in Fig. 3, Dox (10 μM at 1 h) signals were concentrated in the nucleus but displayed less in the cytoplasm in free Dox-treated cancer cells; however, in Dox-gluRDVs-DiD-treated cancer cells, the Dox signals were localized predominantly in the cytoplasm rather than the nucleus. Moreover, the cytoplasmic Dox signals were shown to be mainly colocalized with LysoTracker Blue DND-22 (blue) staining for lysosomes to display merged purple signals, indicating that in Dox-gluRDVs-DiD-treated cancer cells cytoplasmic Dox likely located in acidic lysosome compartments. Interestingly, the few cytoplasmic Dox signals were also shown to be located in lysosomes indicated by merged purple signals in free Dox-treated cancer cells, but Dox-gluRDVs-DiD-treated cancer cells displayed much stronger purple signals than free Dox-treated cancer cells because the most of Dox enriched in lysosomes in Dox-gluRDVs-DiD-treated cancer cells. In addition, the confocal images showed that Dox-gluRDVs-DiD-treated TOV21G cells displayed cytoplasmic DiD signals (green) away from lysosomal Dox fluorescence (red) (Fig. 3E), demonstrating the separate uptake of conjugated Dox and gluRDVs-DiD in TOV21G cells as observed in Supplementary Fig. S2E. These results suggested that Dox-gluRDVs released and transported their conjugated Dox through different pathway from that of free Dox, resulting in distinct subcellular localizations of conjugated/released Dox with cytoplasmic (lysosomal) prevalence from free Dox with nuclear prevalence (Fig. 3A–E and Supplementary Fig. S4A). Moreover, the data suggested the involvement of gluRDVs-mediated redistribution of intracellular Dox in gluRDVs-enhanced antitumor activity.

ROS generation

We next investigated whether the lysosomal Dox could induce oxidative stress in Dox-gluRDVs-treated cancer cells. In B16F10 and TOV21G cells, gluRDVs and free Dox induced a minor increase of DCF fluorescence. In HT-29 and PC3 cells, a weak increase of DCF fluorescence was observed with free Dox but not gluRDVs. Neither gluRDVs nor free Dox could induce significant increase of DCF fluorescence in MES-SA cells. Although Dox has been reported to be able to stimulate ROS production in various cancer cells [13–15] our results suggested that free Dox at low dose inefficiently induce significant ROS production in these cancer cell lines. However, incubation with Dox-gluRDVs showed marked increases of DCF fluorescence in all cancer cell lines (Fig. 3F and Supplementary Fig. S4B), suggesting that enriched lysosomal Dox could induce intracellular oxidative stress in Dox-gluRDVs-treated cancer cells. Although we could not conclude the precise role of lysosomal Dox-mediated ROS in the elevated cytotoxicity of Dox-gluRDVs (Supplementary Fig. S5), these results that Dox-gluRDVs could more efficiently induce ROS generation than free Dox suggested the important contribution of ROS overproduction to gluRDVs-enhanced cytotoxicity of Dox.

Lysosomal Dox accumulation followed by mitochondrial ROS generation

Given the fact that the released Dox was enriched and located in lysosomes in all Dox-gluRDVs-DiD-treated cancer cells and Dox-gluRDVs indeed induced ROS overproduction in all the cells (Fig. 3 and Supplementary Fig. S4), these cancer cell lines were simultaneously stained and examined for their lysosomes with LysoTracker Blue DND-22 and mitochondria with MitoTracker Deep Red both indicated in red as well as ROS production with DCFDA and the auto-fluorescence of Dox indicated in green to determine the distribution/production of Dox/ROS. With the incubation time progression, lysosomal Dox signals (merged in yellow noted with yellow arrows) were gradually increasing and markedly showed at 8 h incubation but declined at 12 h incubation in free Dox-treated B16F10 cells (Fig. 4A, top panel), moreover, obvious ROS signals emerged and were localized with MitoTracker Deep Red staining (mitochondria) at 12 h incubation in free Dox-treated B16F10 cells (Fig. 4A, bottom panel). In Dox-gluRDVs-treated B16F10 cells, released Dox signals (noted with yellow arrows) significantly expressed in lysosomes at 4 h incubation but less remained in lysosomes at 8 h incubation, accompanying with more obvious nuclear Dox than 1 h incubation (Fig. 3A), however, lysosomal Dox signals (noted with yellow arrows) largely arose again but nuclear Dox disappeared at 12 h incubation (Fig. 4B, top panel). Furthermore, ROS signals were remarkably generated at 8 h incubation and immensely visualized at 12 h incubation, and colocalized with mitochondria (Fig. 4B, bottom panel). In free Dox-treated HT-29 cells, lysosomal Dox signals arose faintly at 4 h incubation and were getting increased with incubation time progression (Fig. 4C, top panel), along with visible mitochondrial ROS at 8 h incubation and greater ROS production at 12 h incubation (Fig. 4C, bottom panel). In Dox-gluRDVs-treated HT-29 cells, released Dox signals significantly but less remained in lysosomes at 4 h incubation than 1 h incubation (Fig. 3B) but increasingly

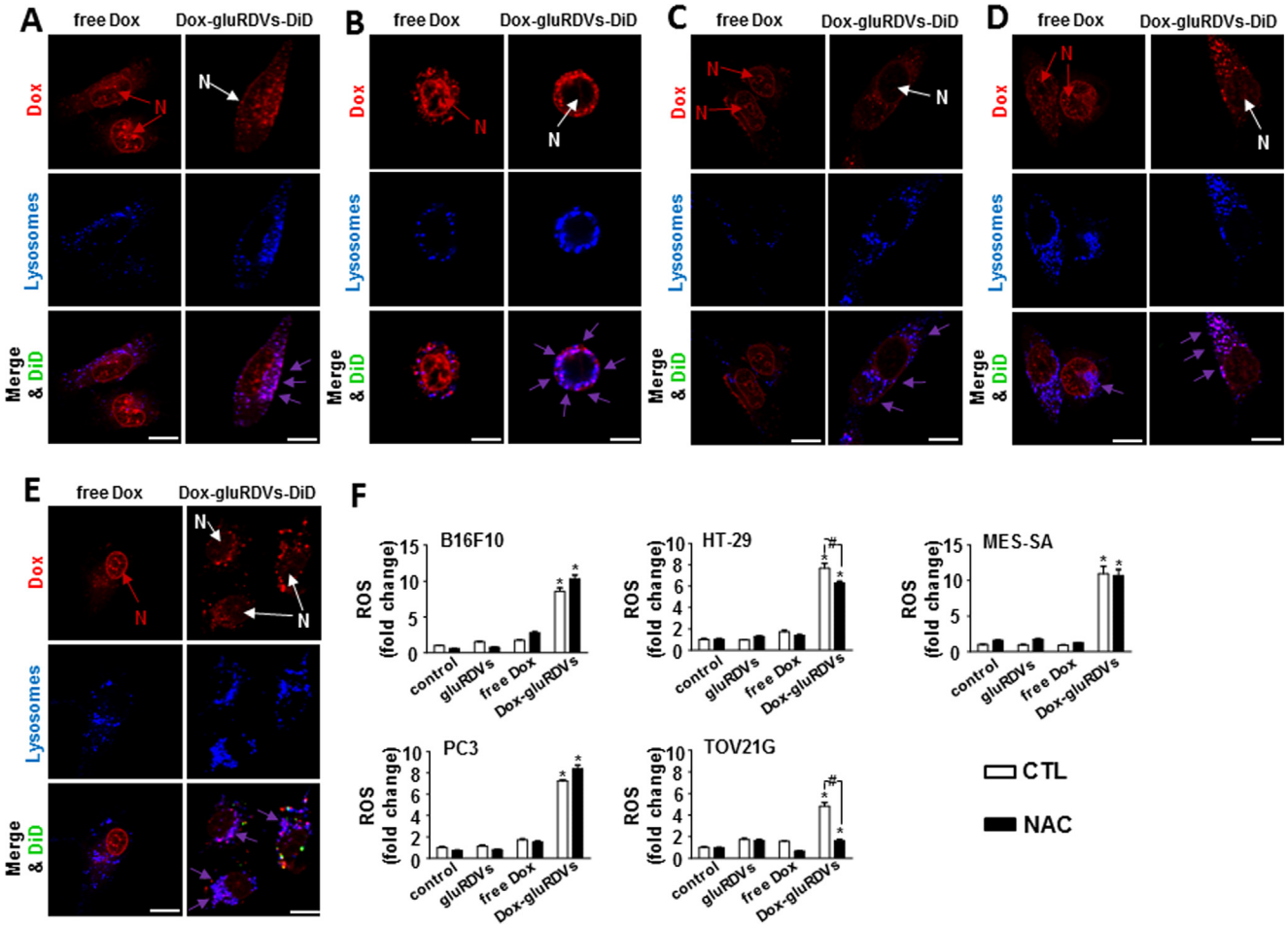

Fig. 3. Intracellular distribution of free Dox and Dox-gluRDVs and ROS generation. (A–E) These cells, including B16F10 cells (A), HT-29 cell (B), MES-SA cells (C), PC3 cells (D), and TOV21G cells (E), were treated with free Dox or Dox-gluRDVs-DiD at equally higher concentration of Dox (10 μM) after 1 h of incubation and then stained with LysoTracker Blue DND-22 (blue). Concentrated Dox in the nucleus (N in red) was marked with red arrow in free Dox-treated cells; in contrast, faint Dox in the nucleus (N in white) was marked with white arrow in Dox-gluRDVs-DiD-treated cells. Colocalization of Dox with lysosome was shown as purple staining marked with purple arrow. Scale bar: 10 μm. (F) Cells, pretreated without (CTL, blank bar) or with NAC (5 mM) (black bar), were treated with vehicle (control), gluRDVs, free Dox or Dox-gluRDVs at equally low concentration of Dox (1 μM) after 24 h of incubation and then stained with DCFDA for flow cytometry assay (*p*-values: * < 0.05 as compared with control; # < 0.05). See supplementary data for detail of Fig. 3.

re-colocalized with lysosomes with incubation time progression, simultaneously accompanying with more accumulated nuclear Dox (Fig. 4D, top panel). The occurrence of mitochondrial ROS happened at 4 h incubation and the incubation time-dependent ROS increase was observed in Dox-gluRDVs-treated HT-29 cells (Fig. 4D, bottom panel). Interestingly, in free Dox-treated MES-SA cells, both lysosomal Dox signals (Fig. 4E, top panel) and mitochondrial ROS (Fig. 4E, bottom panel) were observed at 4 h incubation and enlarged at 8 h incubation but simultaneously declined at 12 h incubation. However, in Dox-gluRDVs-treated MES-SA cells, both lysosomal Dox signals (Fig. 4F, top panel) and mitochondrial ROS (Fig. 4F, bottom panel) were remarkable at 4 h incubation and getting stronger with incubation time progression, nuclear Dox signals seemed to be getting stronger with incubation time progression as well (Fig. 4F, top panel). Moreover, both lysosomal Dox signals and mitochondrial ROS appeared to be much more evident in Dox-gluRDVs-treated MES-SA cells than free Dox-treated MES-SA cells at the same incubation time points (Fig. 4E, top panel vs. Fig. 4F, top panel and Fig. 4E, bottom panel vs. Fig. 4F, bottom panel). In free Dox-treated PC3 cells, lysosomal Dox signals were greatly produced at 4 h and augmented with the incubation time progression (Fig. 4G, top panel), along with visible mitochondrial ROS production at 4 h and profound mitochondrial ROS increase with the incubation time progression (Fig. 4G, bottom panel). Dramatically, in Dox-gluRDVs-treated PC3 cells, immense lysosomal Dox signals retained all the time (Fig. 4H, top panel), moreover, grand mitochondrial ROS was observed at 4 h incubation and much profounder mitochondrial ROS was time-dependent produced (Fig. 4H, bottom panel). In free Dox-treated TOV21G cells, both lysosomal Dox signals (Fig. 4I, top panel) and mitochondrial ROS (Fig. 4I, bottom panel) were significantly observed at 4 h incubation and getting stronger with incubation time progression, however, in Dox-gluRDVs-treated TOV21G cells, tremendous lysosomal Dox signals were maintained at 4 h incubation as compared with 1 h incubation (Fig. 3E), despite they seemed to be decreased instead but still maintained highly remarkable (Fig. 4J, top panel). Interestingly, tremendous mitochondrial ROS was also observed at 4 h incubation and displayed a declined- but still highly expressed-pattern with incubation time progression (Fig. 4J, bottom panel). Our results (Fig. 4 and Supplementary Fig. S6) indicated that free Dox and Dox-gluRDVs' Dox would be mostly distributed between lysosomes and nucleus but Dox-gluRDVs displayed much greater efficiency in lysosomal Dox accumulation than free Dox did and the intracellular ROS was mainly generated in mitochondria but not in Dox-existing lysosomes (Supplementary Fig. S7). Because in all tested cancer cells, no matter

with free Dox or Dox-gluRDVs treatment, the lysosomal Dox distribution always preceded the ROS production, we suggested that the accumulation of lysosomal Dox to an adequate concentration threshold, in spite of either free Dox or released Dox from Dox-gluRDVs, could subsequently cause the mitochondrial ROS production through unrevealed mechanisms in the present study. Although the distribution ratio of free Dox and Dox-gluRDVs-released Dox between lysosomes and nucleus and the consequent ROS production rate varied depending on the cell type, Dox-gluRDVs could more efficiently and promptly deliver their released Dox into lysosomes than free Dox, and hence Dox-gluRDVs could more quickly induce much more mitochondrial ROS than free Dox, suggesting that Dox localization in lysosomes or/and lysosomal Dox-caused ROS indeed played the critical role for the superior cytotoxicity of Dox-gluRDVs but the secondary role of nuclear-targeting function of release Dox also existed in Dox-gluRDVs-treated cells.

By contrast, large amount of free Dox in the cell nucleus indicated the nuclear-targeting function mainly responsible for the cytotoxicity of Dox in free Dox-treated cells, however, free Dox, along with Dox incubation time progression, was also shown to increasingly localize in lysosomes followed by the time-dependent increase of ROS in mitochondria, suggesting that the contribution of lysosomal Dox to the cytotoxicity of Dox in free Dox-treated cells could not be excluded (Supplementary Fig. S8).

Lysosomal membrane permeabilization (LMP) and mitochondrial membrane potential ($\Delta\psi m$) loss

Due to the enriched lysosomal Dox and the consequently much more mitochondrial ROS production in Dox-gluRDVs-treated cancer cells than free Dox-treated cancer cells, we wondered whether these lysosomal Dox in Dox-gluRDVs-treated cancer cells could induce lysosome-dependent cell death (LCD) or ROS could induce the loss of mitochondrial membrane potential ($\Delta\psi m$). LCD is initiated primarily by lysosomal membrane destabilization or lysosomal membrane permeabilization (LMP), which allows the release of lysosomal contents into the cytosol and is considered to be acting either an initiator or amplifier of lysosomal death pathway. Although the precise molecular mechanisms responsible for LMP are not completely understood, various stimuli have been reported to be able to induce LMP and lead to subsequent LCD via different mechanisms [16–18]. It is known that ROS can induce LMP primarily via peroxidation of membrane lipids. Particularly the lysosomal membrane is prone to ROS-mediated damage because of the lysosomal iron content, which can produce intra-lysosomal ROS via the Fenton reaction [18–20]. Moreover, certain stimuli can generate the production of ROS inside lysosomes [18,21], although the initial burst of ROS is most likely generated by destabilized mitochondria [18,22]. In addition, because of increased metabolic demands, resulting in lysosomal alterations in cancer cells, it is acceptable to

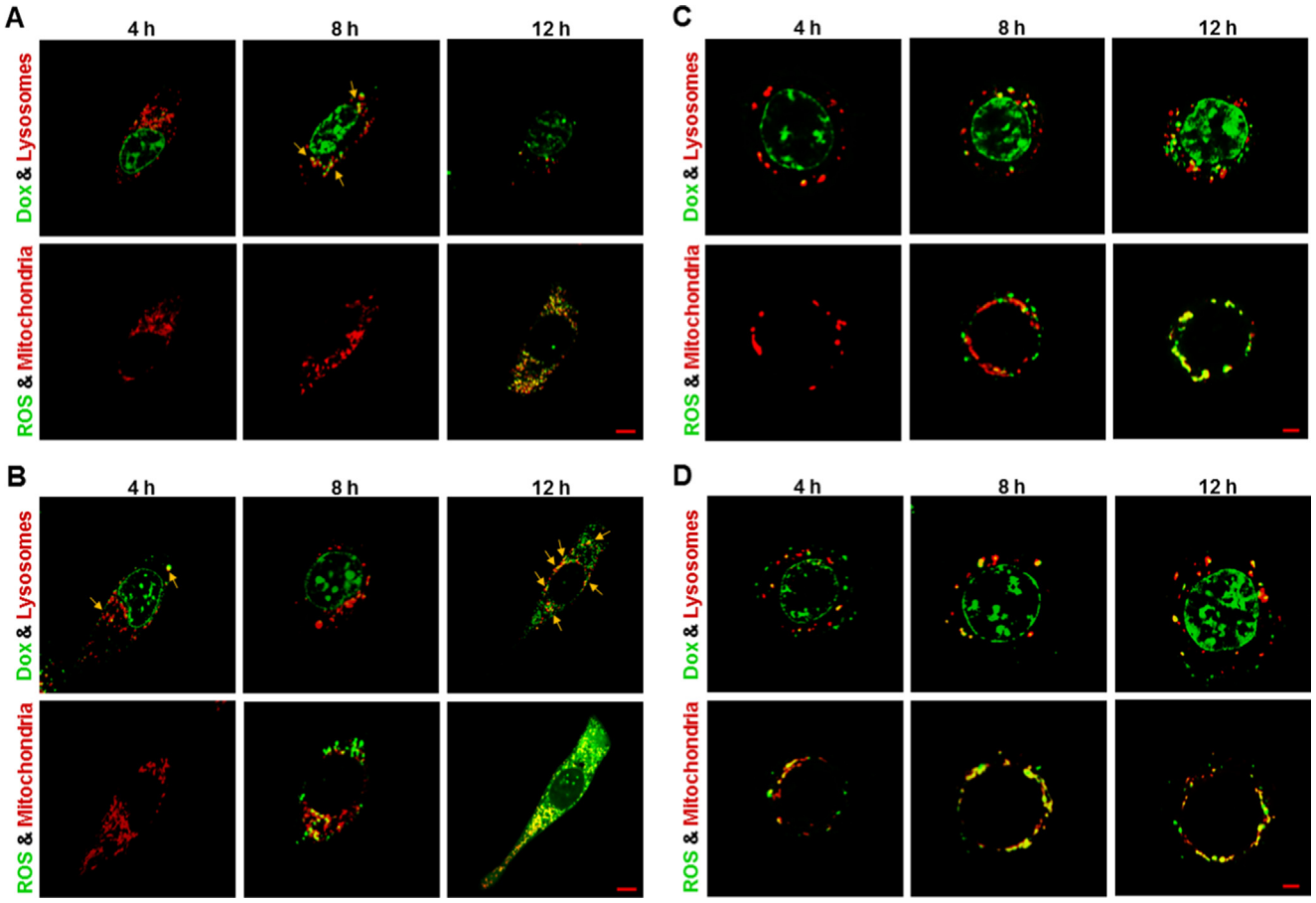

Fig. 4. Lysosomal Dox accumulation followed by mitochondrial ROS generation. Cells, including B16F10 cells (A, B), HT-29 cells (C, D), MES-SA cells (E, F), PC3 cells (G, H), and TOV21G cells (I, J), were treated with free Dox (A, C, E, G, and I) or Dox-gluRDVs (B, D, F, H, and J) at equally higher concentration of Dox (10 μM) at 4 h, 8 h, and 12 h of incubation (Dox signal was designed as shown in green), followed by DCFDA staining for ROS generation (green) and then co-stained with LysoTracker Blue DND-22 (designed as shown in red) and MitoTracker Deep Red (red). Colocalizations of Dox with lysosome, and ROS with mitochondria were shown as yellow staining. Scale bar: 5 μm. See supplementary data for detail of Fig. 4.

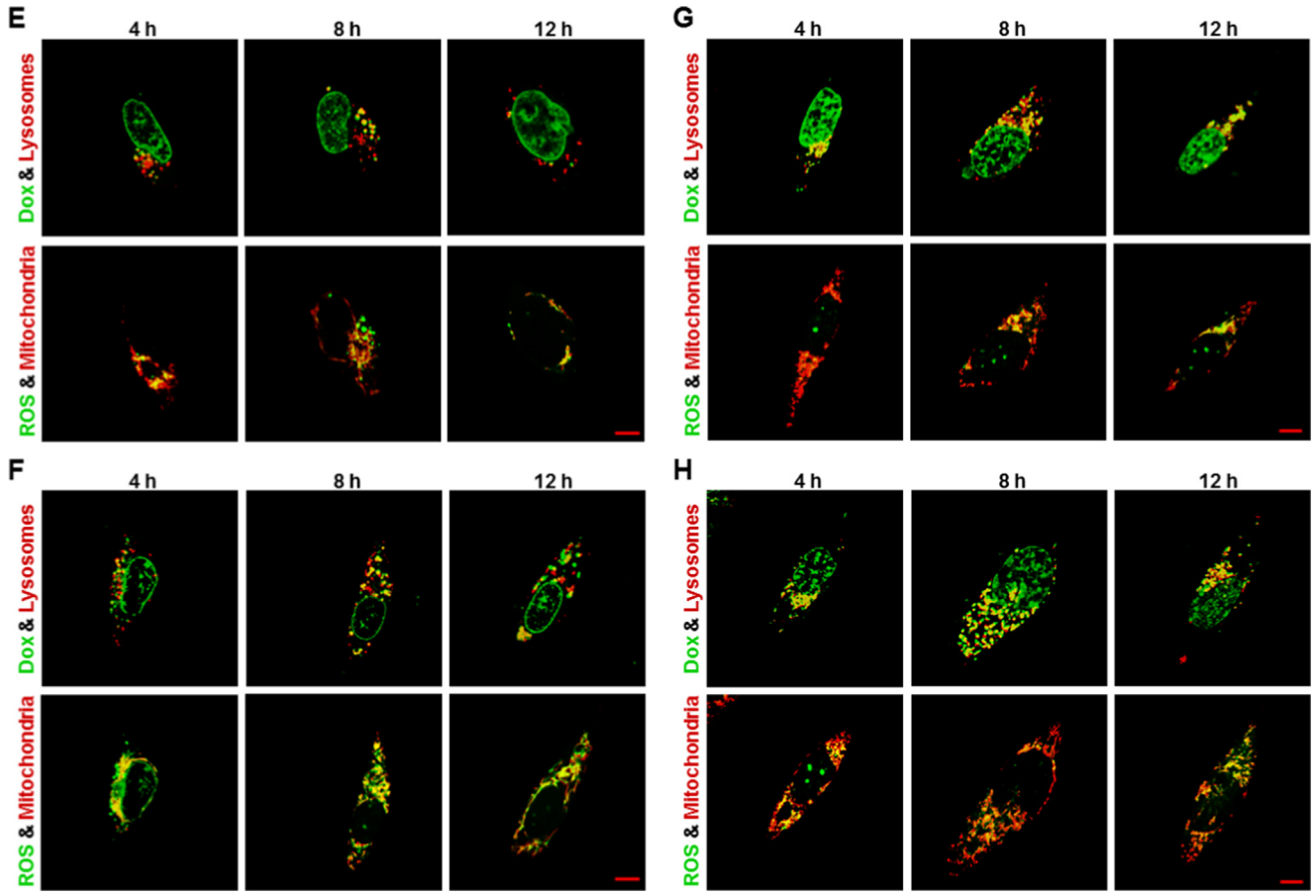

Fig. 4 (*continued*)

propose that cancer cells are more susceptible to LMP-associated LCD than normal cells [16,17]. Basic drugs can accumulate in lysosomes and result in LMP and LCD [23,24]. Several reports indicate that anticancer agents can target lysosomes and induce LMP to lead LCD, either as the major cytotoxicity mechanism or partially contributing to the overall cytotoxicity [16]. Upon LMP, cathepsins (e.g., cathepsins B and D) release from the lysosomal lumen has been proposed to be critical for LCD [17,25,26] and, therefore, can be a determiner of LMP. Until now, to our knowledge, there is no report about the induction of LMP mediated by lysosomal accumulation of Dox or Dox-induced ROS, although an increased expression of cathepsin B but not cathepsins D and L was induced in Dox-treated cancer cells and required for Dox-induced cell death [27]. However, neither cathepsins D release from lysosomes nor acridine orange (AO) fluorescence shift [28] could be observed (data not shown), indicating no LMP or lysosomal membrane destabilization was induce by free Dox or Dox-gluRDVs, which suggested that LMP-associated LCD might not be involved in Dox-gluRDVs-enhanced cytotoxicity.

ROS-mediated mitochondrial dysfunction is an important pathway for inducing cell death. To determine whether mitochondrial dysfunction was involved in Dox-gluRDVs-enhanced cytotoxicity, we measured $\Delta\psi m$ in all tested cancer cells using Rhodamine-123 (Rh-123) as a fluorescent probe. Compared to control cells or free Dox-treated cells, Dox-gluRDVs-treated cells became rounder and shrunk as well as exhibited significantly reduced Rh-123 fluorescence in each of all cancer cell lines (Fig. 5A and Supplementary Fig. S9A). Also, as shown in Fig. 5B and Supplementary Fig. S9B, by using flow cytometry to quantify $\Delta\psi m$, Dox-gluRDVs significantly decreased $\Delta\psi m$ in all tested cells, but not free Dox did. Thus, the data demonstrated that rather Dox-gluRDVs than free Dox caused mitochondrial dysfunction likely mediated by ROS overproduction, which appeared to play the critical role for the superior cytotoxicity of Dox-gluRDVs.

As mentioned above, lysosomes can offer an anticancer target for a number of agents mediated by lysosomal membrane permeability or lysosomal disruption. More recently, a new 'drug free' strategy to kill cancer cells through controlling the aggregation state of otherwise inert Au nanoparticles in lysosomes has been reported [29,30]. However, in contrast to LMP-induced LCD, cancer cells develop mechanisms to inhibit LMP and to evade LCD by modifying their lysosomes [17], moreover, cumulative evidence demonstrate that lysosomes play an important role in hydrophobic weak base chemotherapeutic drug resistance via lysosomal sequestration [31–33]. Lysosomal sequestration of anticancer drugs, such as Dox, resulting in their marked accumulation and compartmentalization in lysosomes, can significantly affect their subcellular distribution and hinder their access to their target sites, thereby to lower their ability to exert a cytotoxic effect [33–35]. Additional report suggests that lysosomal accumulation of anticancer drugs trigger exocytosis of the lysosomal content [36]. Thus, our findings suggested that the released Dox of Dox-gluRDVs, but not free Dox, could be efficiently internalized into lysosomes to be able to overcome lysosomal extrusion via exocytosis, which provide a novel strategy, lysosomal-mitochondrial axis-dependent cancer cell death, to target lysosomes with doxorubicin delivery but instead through mitochondrial ROS overproduction to kill cancer cells without lysosomal damage.

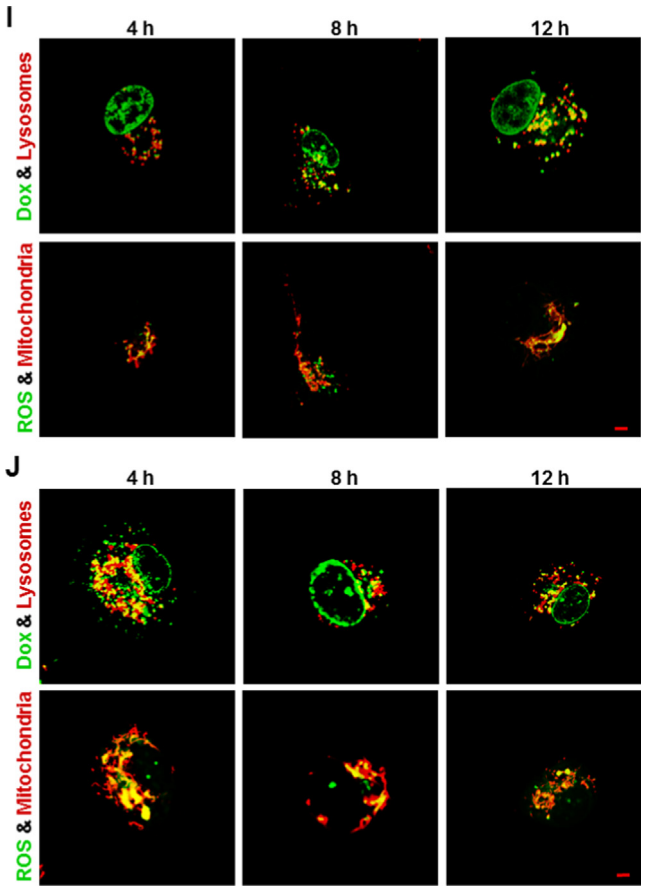

Fig. 4 (*continued*)

Activation of apoptotic signaling

Although several reports have demonstrated the important role of ROS in Dox-induced cancer cell killing, it is still somewhat controversial that other studies did not support the role of ROS in cancer cell death induced by Dox and other chemotherapeutic drugs [37,38]. Considering the role of ROS in Dox-induced cancer cell killing, the extracellular signal-regulated kinase (ERK) has been reported to be upregulated in response to DNA-damaging chemotherapeutic agents, such as Dox, and the activation of the ERK pathway has been considered to correlate with increased cell death [36,37]. In addition, the ERK activation requires ROS production to induce cell death, whereas ERK activity in cell death could be responsible for ROS production [39–41]. Moreover, it has been reported that the activation of caspase-3, a key factor in the execution of apoptosis, is involved in Dox-induced ROS-mediated cancer cell killing [12,13], and ERK activity has been involved in activation of caspase-3 [39,40]. We therefore investigated the effects of free Dox and Dox-gluRDVs on the activation of ERK and caspase-3. We found that Dox-gluRDVs but not free Dox treatment resulted in dramatic ERK activation (phosphorylation) in all cancer cells and that free Dox induced either none or weak of the appearance of cleaved isoform of caspase-3 (cleaved caspase-3), however, Dox-gluRDVs indeed caused much stronger increase of cleaved caspase-3 than free Dox in all tested cancer cells (Fig. 5C and Supplementary Fig. S9C). The much stronger effects of Dox-gluRDVs than free Dox on the activation of ERK and caspase-3, mitochondrial dysfunction, mitochondrial ROS production, and lysosomal localization/accumulation showed the great consistence in all cancer cells, suggesting that the activation of ERK and caspase-3 might act as the crucial signaling responsible for lysosomal Dox-caused ROS overproduction-mediated mitochondria-dependent cell death.

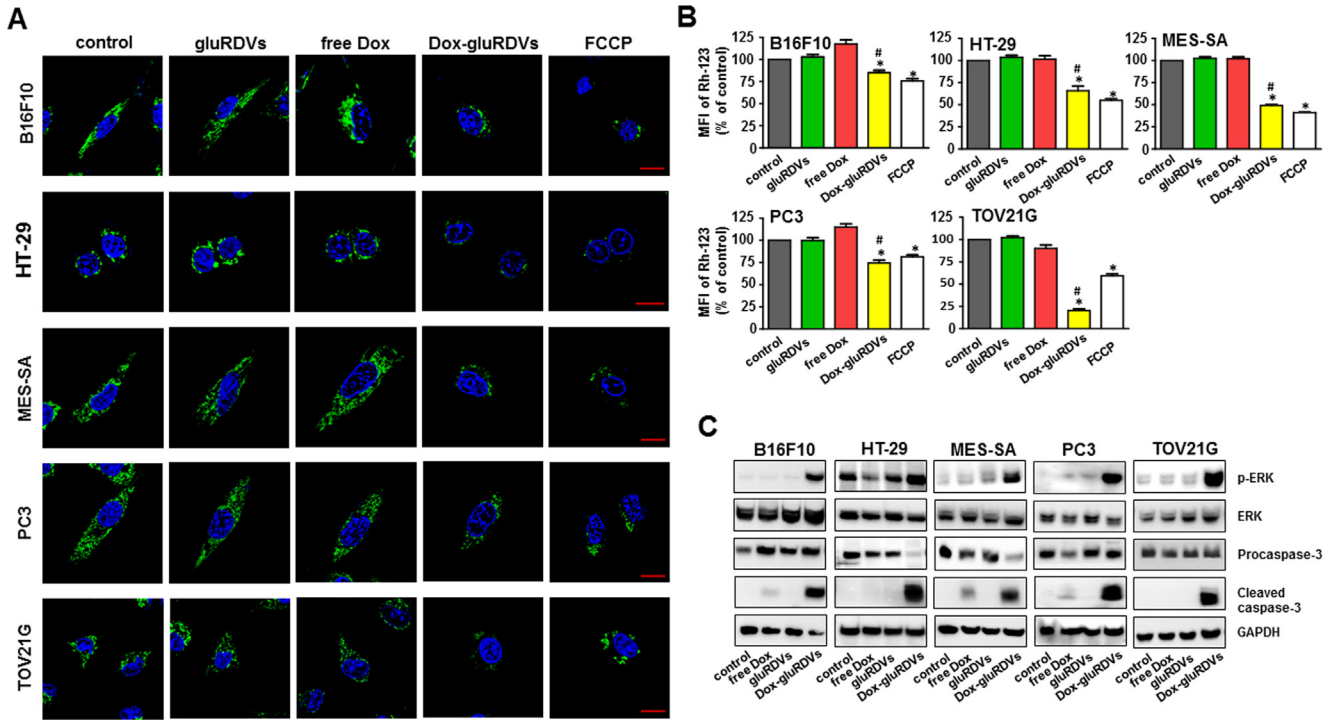

Fig. 5. Mitochondria membrane potential (Δψm) loss and activation of apoptotic signaling. (A, B) Cells were treated with vehicle (control), gluRDVs, free Dox, Dox-gluRDVs at equally higher concentration of Dox (10 μM) or FCCP (100 μM as positive treatment) after 8 h of incubation and then stained with Rh-123 for microscopic observation (A) and flow cytometry (B). (A) Rh-123 staining for mitochondrial membrane potential. Reduced Rh-123 fluorescence (green) was shown in Dox-gluRDVs-treated cells. Hoechst33342 staining for nucleus (blue). Scale bar: 10 μm. (B) Flow cytometry quantification of Δψm presented by mean fluorescence intensity (MFI) of Rh-123 (*p*-values: * < 0.05 as compared with control; # < 0.05 as compared with free Dox). (C) Cells were treated with vehicle (control), gluRDVs, free Dox or Dox-gluRDVs at equally lower concentration of Dox (0.3 μM) after 24 h of incubation and then processed for western blot analysis of ERK phosphorylation and active caspase-3. GAPDH as internal control.

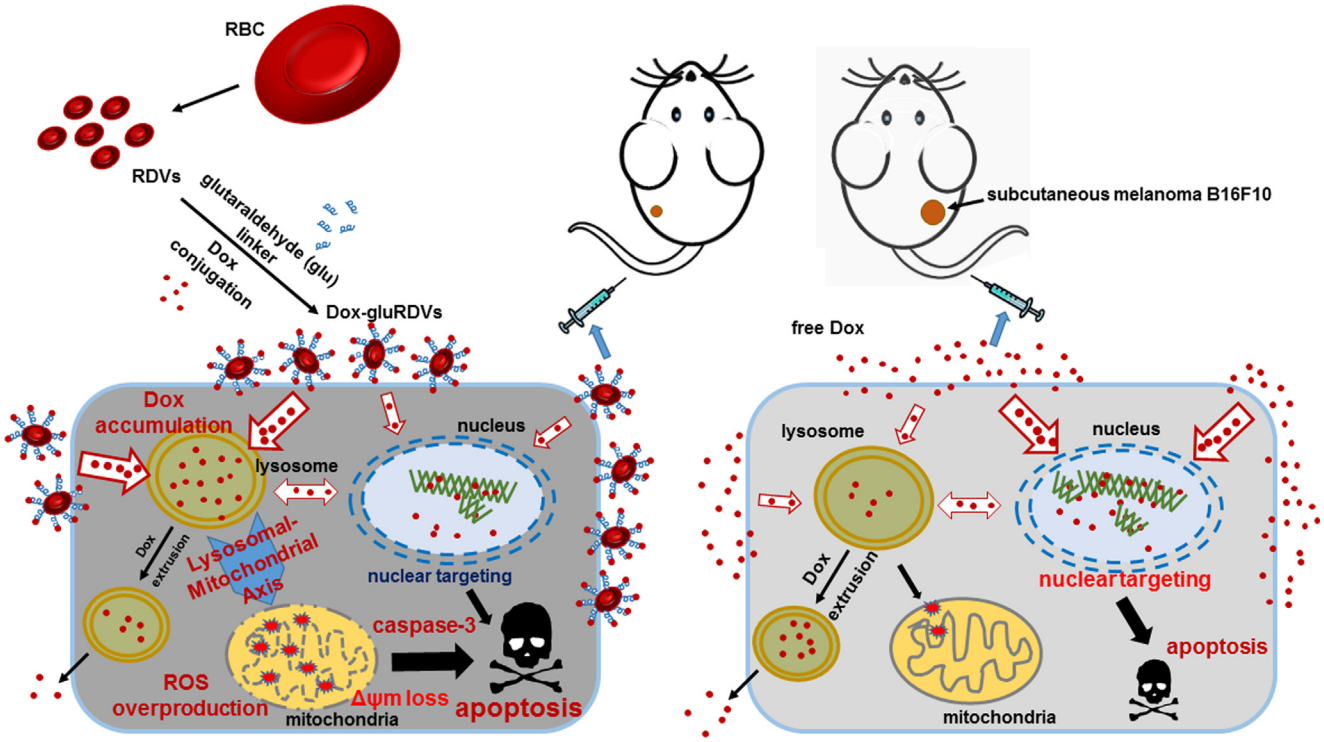

Fig. 6. Schematic illustration of the superior anticancer activity of Dox-gluRDVs. A systemic bDDS (RDVs) of doxorubicin is developed for improved cancer therapy. The as-synthesized Dox-gluRDVs demonstrated superior *in vivo* anticancer activity in subcutaneous melanoma B16F10-bearing mice through intravenous administration. A novel lysosomal-mitochondrial axis-dependent cell death mechanism is revealed: Dox-gluRDVs can efficiently deliver Dox into lysosomes, resulting in the accumulation of adequate quantities of Dox to consequently fuel the mitochondrial ROS overproduction, and subsequently resulting in mitochondrial membrane potential loss and apoptotic activation, which is responsible for superior anticancer activity of Dox-gluRDVs *in vitro* and *in vivo*.

Conclusion

In summary, we have developed a systemic bDDS of doxorubicin (Dox-gluRDVs) for improved cancer therapy. The as-synthesized Dox-gluRDVs demonstrated superior *in vitro* cytotoxicity on a panel of cancer cell lines and enhanced *in vivo* anticancer activity in subcutaneous melanoma B16F10-bearing mice through intravenous administration. Interestingly, *in vitro* novel mechanism (Fig. 6) showed that the superior cytotoxicity of Dox-gluRDVs was not attributed to cellular uptake enhancement but the preference for intracellular distribution of Dox-gluRDVs' released Dox into lysosomes instead. Distinct from free Dox, Dox-gluRDVs can efficiently deliver Dox into lysosomes, resulting in the accumulation of adequate quantities of Dox to consequently fuel the mitochondrial ROS overproduction, and subsequently resulting in mitochondrial membrane potential loss and apoptotic activation, which is responsible for superior anticancer activity of Dox-gluRDVs *in vitro* and *in vivo*. Overall, this work can not only verify that RDVs provide a biocompatible material to improve conventional cancer chemotherapeutics, but also offer a new thought to develop the efficient cancer therapeutic through lysosome-mediated mitochondrial ROS overproduction, a new strategy of lysosomal-mitochondrial axis-dependent cancer cell death.

Compliance with ethics requirements

All procedures followed were in accordance with the ethical standards of the responsible committee on human experimentation (institutional and national) and with the Helsinki Declaration of 1975, as revised in 2008 (5). Informed consent was obtained from all patients for being included in the study.

All Institutional and National Guidelines for the care and use of animals (The Institutional Animal Care and Use Committee (IACUC) of NHRI (NHRI-IACUC), Taiwan) were followed.

Declaration of Competing Interest

The authors declare that they have no known competing financial interests or personal relationships that could have appeared to influence the work reported in this paper.

Acknowledgements

This research was supported by grants from the National Health Research Institutes (NHRI) (BN107-PP-22, BN108-PP-22, and BN109-PP-22), Taiwan.

Appendix A. Supplementary data

Supplementary data to this article can be found online at https://doi.org/10.1016/j.jare.2020.11.009.

References

[1] Kumari P, Ghosh B, Biswas S. Nanocarriers for cancer-targeted drug delivery. J Drug Target 2016;24:179–91.
[2] Villa CH, Anselmo AC, Mitragotri S, Muzykantov V. Red blood cells: supercarriers for drugs, biologicals, and nanoparticles and inspiration for advanced delivery systems. Adv Drug Deliv Rev 2016;106:88–103.
[3] Tan S, Wu T, Zhang D, Zhang Z. Cell or cell membrane-based drug delivery systems. Theranostics 2015;5:863–81.
[4] Villa CH, Seghatchian J, Muzykantov. Drug delivery by erythrocytes: "primum non nocere". Transfus Apher Sci 2016;55:275–80.

[5] Lejeune A, Moorjani M, Gicquaud C, Lacroix J, Poyet P, Gaudreault R. A new derivative of erythrocyte ghost: preparation and antineoplastic potential as drug carrier for daunorubicin. Anticancer Res 1994;14:915–9.
[6] Désilets J, Lejeune A, Mercer J, Gicquaud C. A new derivative of erythrocyte ghost: IV. fate of reinjected nanoerythrosomes. Anticancer Res 2001;21:1741–7.
[7] Chiarantini L, Johnson J, DeLoach JR. Optimized recirculation survival of mouse carrier erythrocytes. Blood Cells 1991;17:607–17.
[8] Hu CM, Zhang L, Aryal S, Cheung C, Fang RH. Erythrocyte membrane-camouflaged polymeric nanoparticles as a biomimetic delivery platform. Proc. Natl. Acad. Sci. USA 2011;108:10980–5.
[9] Gao W, Hu CM, Fang RH, Luk BT, Su J, Zhang L. Surface functionalization of gold nanoparticles with red blood cell membranes. Adv Mater 2013;25:3549–53.
[10] Wang LY, Shi XY, Yang CS, Huang DM. Versatile RBC-derived vesicles as nanoparticle vector of photosensitizers for photodynamic therapy. Nanoscale 2013;5:416–21.
[11] Chang M, Hsiao JK, Yao M, Chien LY, Hsu SC, Ko BS, et al. Homologous RBC-derived vesicles as ultrasmall carriers of iron oxide for magnetic resonance imaging of stem cells. Nanotechnology 2010;21:235103.
[12] Wang S, Konorev EA, Kotamraju S, Joseph J, Kalivendi S, Kalyanaraman B. Doxorubicin induces apoptosis in normal and tumour cells via distinctly different mechanisms: intermediacy of H2O2- and p53-dependent pathways. J Biol Chem 2004;279:25535–43.
[13] Tsang WP, Chau SPY, Kong SK, Fung KP, Kwok TT. Reactive oxygen species mediate doxorubicin induced p53-indipendnet apoptosis. Life Sci 2003;73:2047–58.
[14] Gouazé V, Mirault ME, Carpentier S, Salvayre R, Levade T, Andrieu-Abadie N. Glutathione peroxidase-1 overexpression prevents ceramide production and partially inhibits apoptosis in doxorubicin-treated human breast carcinoma cells. Mol Pharmacol 2001;60:488–96.
[15] Mai Y, Yu JJ, Bartholdy B, Xu-Monette ZY, Knapp EE, Yuan F, et al. An oxidative stress-based mechanism of doxorubicin cytotoxicity suggests new therapeutic strategies in ABC-DLBCL. Blood 2016;128:2797–807.
[16] Domagala A, Fidyt K, Bobrowicz M, Stachura J, Szczygiel K, Firczuk M. Typical and atypical inducers of lysosomal cell death: a promising anticancer strategy. Int J Mol Sci 2018;19:2256.
[17] Halaby R. Role of lysosomes in cancer therapy. Res Rep Biol 2015;6:147–55.
[18] Repnik U, Česen MH, Turk B. Lysosomal membrane permeabilization in cell death: concepts and challenges. Mitochondrion 2014;19:49–57.
[19] Ollinger K, Brunk UT. Cellular injury induced by oxidative stress is mediated through lysosomal damage. Free Radic Biol Med 1995;19:565–74.
[20] Kurz T, Eaton JW, Gustafsson B, Brunk UT. Lysosomes in iron metabolism, aging and apoptosis. Histochem Cell Biol 2008;12:389–406.
[21] Denamur S, Tyteca D, Marchand-Brynaert J, Van Bambeke F, Tulkens PM, Courtoy PJ, et al. Role of oxidative stress in lysosomal membrane permeabilization and apoptosis induced by gentamicin, and aminoglycoside antibiotic. Free Radic Biol Med 2011;51:1656–65.
[22] Turrens JF. Mitochondrial formation of reactive oxygen species. J Physiol 2003;552:335–44.
[23] Logan R, Funk RS, Axcell E, Krise JP. Drug-drug interactions involving lysosomes: mechanisms and potential clinical implications. Expert Opin Drug Metab Toxicol 2012;8:943–58.
[24] Barbosa CM, Oliveira CR, Nascimento FD, Smith MC, Fausto DM, Soufen MA, et al. Biphosphinic palladacycle complex mediates lysosomal-membrane permeabilization and cell death in K562 leukaemia cells. Eur J Pharmacol 2006;542:37–47.
[25] Boya P, Andreau K, Poncet D, Zamzami N, Perfettini JL, Metivier D, et al. Lysosomal membrane permeabilization induces cell death in a mitochondrion-dependent fashion. J Exp Med 2003;197:1323–34.
[26] Emert-Sedlak L, Shangary S, Rabinovitz A, Miranda MB, Delach SM, Johnson DE. Involvement of cathepsin D in chemotherapy–induced cytochrome c release, caspase activation, and cell death. Mol Cancer Ther 2005;4:733–42.
[27] Bien S, Rimmbach C, Neumann H, Niessen J, Reimer E, Ritter CA, et al. Doxorubicin-induced cell death requires cathepsin B in HeLa cells. Biochem Pharmacol 2010;80:1466–77.
[28] Zhao M, Eaton JW, Brunk UT. Bcl-2 phosphorylation is required for inhibition of oxidative stress-induced lysosomal leak and ensuing apoptosis. FEBS Lett 2001;509:405–12.
[29] Borkowska M, Siek M, Kolygina DV, Sobolev YI, Lach S, Kumar S, et al. Targeted crystallization of mixed-charge nanoparticles in lysosomes induces selective death of cancer cells. Nat Nanotechnol 2020;15:331–41.
[30] Qui J, Xia Y. Killing cancer cells by rupturing their lysosomes. Nat Nanotechnol 2020;15:252–3.
[31] Herlevsen M, Oxford G, Owens CR, Conaway M, Theodorescu D. Depletion of major vault protein increases doxorubicin sensitivity and nuclear accumulation and disrupts its sequestration in lysosomes. Mol Cancer Ther 2007;6:1804–13.
[32] Zhitomirsky B, Assaraf YG. Lysosomal sequestration of hydrophobic weak base chemotherapeutics triggers lysosomal biogenesis and lysosome-dependent cancer multidrug resistance. Oncotarget 2015;6:1143–56.
[33] Zhitomirsky B, Assaraf YG. Lysosomes as mediators of drug resistance in cancer. Drug Resist Update 2016;24:23–33.
[34] Duvvuri M, Krise JP. Intracellular drug sequestration events associated with the emergence of multidrug resistance: a mechanistic review. Front Biosci 2005;10:1499–509.
[35] Kazmi F, Hensley T, Pope C, Funk RS, Loewen GJ, Buckley DB, et al. Lysosomal sequestration (trapping) of lipophilic amine (cationic amphiphilic) drugs in immortalized human hepatocytes (Fa2N-4 cells). Drug Metab Dispos 2013;41:897–905.
[36] Zhitomirsky B, Assaraf YG. Lysosomal accumulation of anticancer drugs triggers lysosomal exocytosis. Oncotarget 2017;8:45117–38.
[37] Abrams SL, Steelman LS, Shelton JG, Wong EWT, Chappell WH, Bäsecke J, et al. The Raf/MEK/ERK pathway can govern drug resistance, apoptosis and sensitivity to targeted therapy. Cell Cycle 2010;9:1781–91.
[38] Sapio L, Sorvillo L, Illiano M, Chiosi E, Spina A, Naviglio S. Inorganic phosphate prevents Erk1/2 and Stat3 activation and improves sensitivity to doxorubicin of MDA-MB-231 breast cancer cell. Molecules 2015;20:15910–28.
[39] Lee ER, Kang YJ, Kim JH, Lee HT, Cho SG. Modulation of apoptosis in HaCaT keratinocytes via differential regulation of ERK signalling pathway by flavonoids. J Biol Chem 2005;280:31498–507.
[40] Matsunaga Y, Kawai Y, Kohda Y, Gemba M. Involvement of activation of NADPH oxidase and extracellular signal-regulated kinase (ERK) in renal cell injury induced by zinc. J Toxicol Sci 2005;30:135–44.
[41] Zhang X, Shan P, Sasidhar M, Chupp GL, Flavell RA, Choi AM, et al. Reactive oxygen species and extracellular signal-regulated kinase 1/2 mitogen-activated protein kinase mediate hyperoxia induced cell death in lung epithelium. Am J Respir Cell Mol Biol 2003;28:305–15.